

Journal of Experimental Psychology: Human Perception and Performance

Anticipation in Manual Tracking With Multiple Delays

Nigel Stepp and Michael T. Turvey

Online First Publication, February 23, 2017. <http://dx.doi.org/10.1037/xhp0000393>

CITATION

Stepp, N., & Turvey, M. T. (2017, February 23). Anticipation in Manual Tracking With Multiple Delays. *Journal of Experimental Psychology: Human Perception and Performance*. Advance online publication. <http://dx.doi.org/10.1037/xhp0000393>

Anticipation in Manual Tracking With Multiple Delays

Nigel Stepp

HRL Laboratories, LLC, Malibu, California

Michael T. Turvey

University of Connecticut and Haskins Laboratories,
New Haven, Connecticut

Two experiments are reported showing that behavior exhibited in manual tracking is consistent with behavior predicted by a dynamical systems phenomenon known as anticipating synchronization (Voss, 2000). They extend a prior investigation of the effect of delay on anticipatory manual tracking (Stepp, 2009) by also manipulating coupling strength. The coupling scheme in Experiment 1 and that in Experiment 2 go beyond the single delayed feedback coupling used in previous research and articulations of anticipating synchronization. These advanced coupling arrangements are addressed using an extended formulation which allows for multiple feedback delays, a continuous range of delay, or even coupling to real future values. The latter case is specifically investigated in Experiment 2, which utilizes a navigation task that provides a natural way to speak about coupling to future values.

Public Significance Statement

This study suggests that certain kinds of anticipatory behavior can be explained through ubiquitous physical processes. The implication is that anticipation, which seems to ask for a model of the future, might be grounded in a theory without such a model. Doing so alleviates the need to explain the genesis of anticipatory models at such a low level, and provides insight into perception and action as well.

Keywords: tracking, synchronization, anticipation, feedback delay

It is not unreasonable to claim that all organisms in all phyla of all Six Kingdoms (Bacteria, Archaea, Protoctista, Plantae, Fungi, Animalia) exhibit agency, in greater or lesser degree (Turvey, 2013, 2015). That is, they manifest some degree of autonomy and control, *however minimal*, in their encounters. Agency encompasses (a) variation of means to bring about an end (flexibility), (b) coordinating current control with preceding states of affairs (retrospectivity), and (c) coordinating current control with upcoming states of affairs (prospectivity; Gibson, 1994). Commonly, one refers to the retrospective dimension as *memory* and the prospective dimension as *anticipation*. The latter functional ability and what it entails is the present experimental focus.

There is strong evidence that at least some prospective control problems are solved through continuous dynamical coupling. One such problem is the well-studied variant of prospective control in human behavior is the so-called “outfielder problem.” The out-

fielder perceives where he or she must be to intercept the ball by so moving as to maintain invariant the rate of change of the optical expansion of the ball’s optical contour in the ambient optic array at his or her point of observation (e.g., Fink, Foo, & Warren, 2009; Michaels & Oudejans, 1992). The outfielder’s behavior does not entail, as commonly assumed, modeling the ball’s flight via the implicit application of Newton’s laws and physical optics (e.g., Saxberg, 1987).

Previously, Stepp (2009) found that human behavior in a prospective manual tracking task is consistent with behavior predicted by a dynamical systems phenomenon known as anticipating synchronization (Voss, 2000), which describes delayed-feedback induced prospectivity governed by two main parameters, coupling strength and delay. Stepp (2009) investigated the effect of delay on anticipatory manual tracking, but the experimental paradigm did not readily accept manipulation of coupling strength. Experiment 1 is an attempt to rectify this, by varying both delay and strength of coupling. The coupling scheme in Experiment 1 and that in Experiment 2 go beyond the single delayed feedback coupling used in Stepp (2009) and previous formulations of anticipating synchronization. These advanced coupling arrangements are addressed using an extended formulation developed in Stepp and Turvey (2015), which allows for multiple feedback delays, a continuous range of delay, or even coupling to real future values. The latter case is specifically investigated in Experiment 2, which utilizes a navigation task that provides a natural way to speak about coupling to future values.

For Dubois (2003), anticipation is weak if it arises from a model of the system via internal simulations. Anticipation is strong if it arises from the system itself, via lawful regularities embedded in

Nigel Stepp, Information & Systems Sciences Laboratory, HRL Laboratories, LLC, Malibu, California; Michael T. Turvey, Center for the Ecological Study of Perception and Action, University of Connecticut, and Haskins Laboratories, New Haven, Connecticut.

This work was supported in part by National Science Foundation Grant BCS-1344725, and in part by Defense Advanced Research Projects Agency Physical Intelligence subcontract HRL 000708-DS.

Correspondence concerning this article should be addressed to Nigel Stepp, Information & Systems Sciences Laboratory, HRL Laboratories, LLC, 3011 Malibu Canyon Road, Malibu, CA 90265. E-mail: ndstepp@hrl.com

the system's ordinary mode of functioning. (For the outfielder problem, the system is ball-and-outfielder.) The strategic importance of this latter notion is that it invites a shift of focus from theorizing about a *representation-anticipation relation* to theorizing about a *coupling-anticipation relation*. Rather than asking how the future is produced from an internal model (e.g., Rosen, 2012) one asks about a coupling (between organism and environment) that results in coordination with the future (Stepp & Turvey, 2010). The experiments that follow are intended to approach the question of anticipation from this perspective. That is, supposing there is an explanation for certain kinds of anticipatory behavior that does not require appeal to abstractions such as representation, what would those explanations look like? Ideally, they would have the form of law-based dynamical systems.

General Method

In the delay coupling

$$\begin{aligned}\dot{\mathbf{x}} &= f(\mathbf{x}) \\ \dot{\mathbf{y}} &= g(\mathbf{y}) + k(\mathbf{x} - \mathbf{y}_\tau)\end{aligned}\quad (1)$$

as used by Stepp (2009), f and g are intrinsic dynamics of multi-dimensional systems \mathbf{x} and \mathbf{y} , respectively, k is a coupling strength, and \mathbf{y}_τ is $\mathbf{y}(t - \tau)$. In this formulation, we expect anticipating synchronization to obtain when f and g are similar. The exact bounds of similarity are a topic for future study. In the following, we assume both f and g are oscillatory, with characteristic periods that are close enough to allow for at least intermittent frequency locking. In the context of human perception and performance, system \mathbf{x} is taken to be a perceivable, changing feature of the environment, and \mathbf{y} a perception–action system. Stepp and Turvey (2015) detailed a more general formulation of the coupling function that allows description of couplings with more complicated feedback structures. Equation 2 is intended to replace the simple $k(\mathbf{x} - \mathbf{y}_\tau)$ coupling function from Equation 1 with a coupling function that admits arbitrary combinations of past and future feedback. It takes the form:

$$h(\mathbf{x}, \mathbf{y}, t) = \int_0^\infty \int_0^\infty K(s, u)(\mathbf{x}(t + u) - \mathbf{y}(t - s)) ds du \quad (2)$$

Here, u and s are time shifts into future and past, respectively. The coupling strength function K allows different coupling for different shifts. For example, choosing $K(s, u) = k\delta(s - \tau)\delta(u)$, where δ is the Dirac delta function, recovers the coupling function in Equation 1.

We report two experiments that explore this expanded space of delay coupling arrangements. The strength function of the coupling in Experiment 1 was of the form

$$K(s, u) = k\delta(u) \sum_{\tau \in T} \delta(s - \tau) \quad (3)$$

where T is a discrete set of delays. Experiment 2 instantiates a driving task in order to investigate coupling to future values in a workable fashion. In this task, road width under a perspective transform falls off as $\frac{2}{\pi} \arctan \frac{1}{d}$ after distance d . Accordingly, the coupling strength function takes the form

$$K(s, u) = \frac{2}{\pi} \arctan \left(\frac{1}{u} \right) \delta(s - \tau) \quad (4)$$

providing for the full coupling function

$$h(\mathbf{x}, \mathbf{y}, t) = \int_0^\infty \frac{2}{\pi} \arctan \left(\frac{1}{u} \right) (\mathbf{x}(t + u) - \mathbf{y}(t - \tau)) du \quad (5)$$

Equation 5 is a system in which there is a quickly but infinitely diminishing coupling to upcoming values along with self-feedback for a single delay. Although the integral of this choice for $K(s, u)$ diverges, practical and physical limitations would constrain it in practice.

Simulations

Different coupling functions are expected to result in different synchronization behaviors. To envisage what should be expected from the couplings described above, simulations of systems with those couplings were performed.

Stepp and Turvey (2015) introduced a shorthand for denoting classes of coupling function. As u and s represent master and slave time-shifts, respectively, U and S denote their place in the coupling function, with a subscript to denote the multiplicity of time-shift, for example, 0, 1, n , or ∞ for, respectively, current time, one shift, many shifts, or a continuous range. Simulations of the canonical delay-coupling system in Equation 1 have been conducted for the Rössler–Spring system (Stepp, Chemero, & Turvey, 2011; Stepp & Turvey, 2010), and certain features of the resulting dynamics noted. Furthermore, Stepp (2009) saw evidence of these same features in empirical data for another system from the U_0S_1 class.

$$\begin{aligned}\dot{x}_1 &= -x_2 - x_3 \\ \dot{x}_2 &= -x_1 + ax_2 \\ \dot{x}_3 &= b + x_3(x_1 - c) \\ \dot{y}_1 &= y_2 + h(\mathbf{x}, \mathbf{y}, t) \\ \dot{y}_2 &= -y_1\end{aligned}\quad (6)$$

Where a , b , and c are parameters of the Rössler oscillator, and $h(\mathbf{x}, \mathbf{y}, t)$ is a coupling function of the form of Equation 2.

Simulations of U_0S_n

In what follows, we report simulations of a Rössler–Spring system specified by Equation 6 with a coupling function from the U_0S_n class for values of $n \geq 1$, specifically Equation 2 with K given by Equation 7 (see below). The parameters $a = b = 0.1$, $c = 14$ were used for the Rössler and $w = 1$ was used for the spring. Initial conditions of both systems were kept constant between simulations, at $x_1 = 18.68$, $x_2 = 3.432$, $x_3 = 20.9$, $y_1 = 1$, $y_2 = 0$. Simulations were run in MATLAB using the *dde23* delay differential equation solver with a different set of delays or lags for each simulation as described below.

Two dimensions along which a discrete delay set can vary are number of delays and maximum delay. For instance, the delay sets $\{0.3, 0.6\}$ and $\{0.2, 0.4, 0.6\}$ differ in number, but not in maximum value, whereas $\{0.3, 0.6\}$ and $\{0.4, 0.8\}$ differ in maximum value, but not in number. To cover a region in this space of possible delay sets, many simulations were run with maximum delay and feedback count (number of delayed feedback terms) combinations taken from $\tau = \{0.1, 0.2, \dots, 2\}$ s and $n = \{1, 2, \dots, 15\}$. A delay set was constructed for each combination by choosing $n + 1$ equally spaced delays from 0 to τ , then dropping 0. For this collection of simulations, each delayed

feedback term was given equal weight scaled by the number of feedback terms. In terms of Equation 2, the system being simulated is given by

$$K(s, u) = \sum_i^n \frac{1}{n} \delta(s - \tau_i) \delta(u) \quad (7)$$

with τ_i taken from the n -element delay set as constructed above.

Figure 1a shows the maximum cross-correlation measurement (Stepp & Frank, 2009) for each combination of feedback count and maximum delay. This measurement is the highest correlation found at some time shift between two time series. The time shift at which that happens is plotted in Figure 1b. Note that the canonical case is present here for $n = 1$. One clear feature of the plot is that correlation remains high for higher delays when adding more feedback elements. That is, adding more delays stabilizes synchronization—a feature predicted by Atay and Karabacak (2006) who note, “To the extent that multiple delays in maps can be considered as the counterpart of distributed delays, one might anticipate further stabilization effects in such general networks” (p. 523).

Simulations of $U_\infty S_1$

In the simulations, a single delayed feedback is combined with coupling to a continuous section of upcoming values of the master system. This arrangement is not supported explicitly by the *dde23* solver used in previous simulations, which only handles positive delay values. In order to conduct the simulation, a master time series was solved using an ordinary differential equation solver and the solution used within the slave DDE equations to later evaluate future values as needed.

Again, there is a range of possible values for both feedback delay and amount of look-ahead. Rather than taking all upcoming values into account, a section of the master time series is considered. In equation form, the system being studied here is given by

$$K(s, u) = \frac{2}{\pi} \arctan\left(\frac{1}{u}\right) (H(u) - H(u - \tau_m)) \delta(u - \tau_d) \quad (8)$$

or, plugging in to Equation, as an evaluated coupling function,

$$h(\mathbf{x}, \mathbf{y}, t) = \int_0^{\tau_m} \frac{2}{\pi} \arctan\left(\frac{1}{u}\right) (\mathbf{x}(t+u) - \mathbf{y}(t - \tau_d)) du \quad (9)$$

where (τ_m) is taken from the set $\{1, 2, \dots, 8\}$ s and (τ_d) is taken from $\{0.2, 0.4, \dots, 1\}$ s. The ρ and τ^* measures are presented in Figure 2.

Experiment 1

It is clear from previous studies of human manual tracking that tracking can be anticipatory. Delayed feedback puts participants into a position where they must anticipate so as to succeed in the task (Foulkes & Miall, 2000; Vercher & Gauthier, 1992; Voss, McCandliss, Ghajar, & Suh, 2007). The results of Stepp (2009) suggest that this delay-anticipation relation is analogous to the dynamical systems phenomenon of anticipating synchronization (Voss, 2000). State-based synchronization of two dynamical systems x and y might not only be complete ($y(t) \approx x(t)$) or lagged ($y(t) \approx x(t - \tau)$), but also anticipating ($y(t) \approx x(t + \tau)$). Anticipating synchronization, in one form, is instantiated by Equation 1 in which x and y are states of a master and slave system, respectively.

Stepp (2009) showed the dependence of anticipatory tracking on applied delay. In Equation 1, however, feedback delay τ is one of two important coupling parameters, the other being coupling strength k . As the Stepp (2009) paradigm does not easily admit variable coupling strength, a new paradigm was selected. In the new paradigm, feedback is discretized, and coupling strength is assumed to scale with frequency of feedback. The ability to vary k allows exploration of the (k, τ) parameter space.

Discrete feedback additionally allows for dealing with multiple delays. A single delay is covered by the coupling function above, $k(x - y_\tau)$. Allowing for multiple feedback states, each with some delay, the coupling function can be generalized as $U_\infty S_n$ using a discrete sum

$$K(s, u) = \sum_i^n k_i \delta(s - \tau_i) \delta(u) \quad (10)$$

for some number of delays represented by τ_i , and coupling weights k_i .

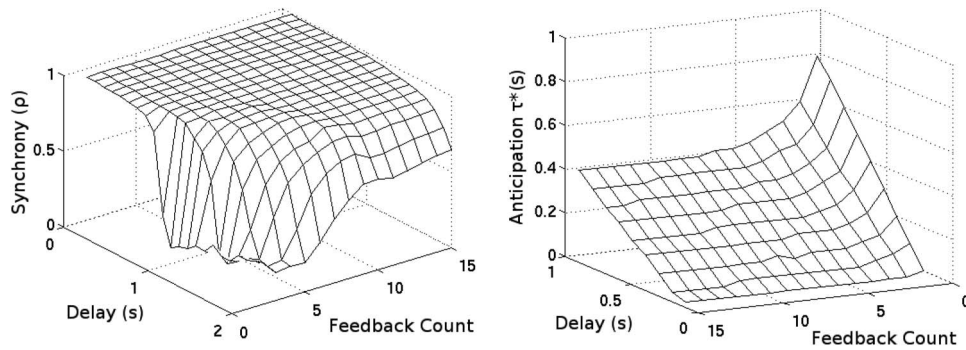


Figure 1. Measurements ρ (left) and τ^* (right) of simulations of coupling class $U_\infty S_n$, which has coupling to the present state of the master, and some number of discrete feedback delays. Maximum delay ranged from 0 to 2 s, and number of equally distributed delays ranged from 1 to 15. In this simulation, each delay was given equal weight.

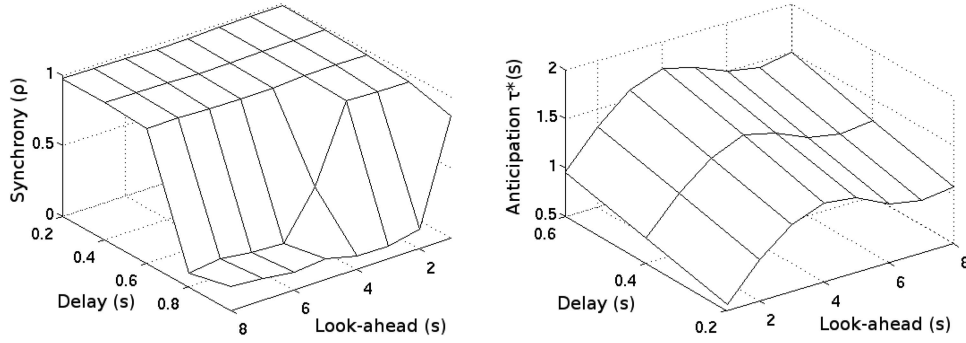


Figure 2. Measurements ρ (left) and τ^* (right) of simulations of coupling class $U_{\infty}S_1$, which has coupling to a continuous region of the master, and a single discrete feedback delay. Feedback delay ranged from 0 to 2 s, and maximum look-ahead time ranged from 1 to 8 s.

Method

Participants. Sixteen students at the University of Connecticut participated in this study. The participants were 7 women and 9 men of which 12 were undergraduate students and 4 were graduate students. Of the 16, 15 were right-handed and one was left-handed, identified by the hand with which the participant preferred to draw. Participants gave informed consent and, in the case of undergraduates, received class credit for their voluntary participation. The study was approved by the University of Connecticut Institutional Review Board.

Design. Each participant viewed a computer display (39 cm diagonal, 800×600 pixel resolution) at a distance of approximately 65 cm from screen to eye. A pressure sensitive tablet (18 cm diagonal) sat 30 cm in front of the same display. The refresh rate of the display was 60 Hz. Participants held a 14 cm stylus in their dominant hand that they could position on the tablet in order to interact with the display. The stylus position was sampled on each screen refresh at a rate of 60 Hz, though it had an intrinsic sampling rate of approximately 100 Hz. The tablet and stylus were visible to the participant, and the background color of the display was set to a light gray color given by RGB triplet (200, 200, 200). A depiction of this setup is shown in Figure 3.

Trials, each lasting 80 s, were organized into 3 blocks of 8 for a total of 24. Typically, there was a 4-s gap between each trial, although participants were able to rest between trials whenever they wished. During each trial a 20×20 pixel blue square, the target, moved along the top of the screen according to a “chaotic spring” function. Specifically, the on-screen s_x coordinate of the trajectory was generated by the x_1 dimension of the system specified by Equation 11.

$$\begin{aligned} \dot{x}_1 &= x_2 \\ \dot{x}_2 &= -\left(2\pi\left(\frac{x_3}{\alpha} + \beta\right)\right)^2 x_1 \\ \dot{x}_3 &= -x_4 - x_5 \\ \dot{x}_4 &= x_3 + ax_4 \\ \dot{x}_5 &= b + x_5(x_3 - c) \end{aligned} \quad (11)$$

This particular system maintains a relatively periodic oscillation, at the same time varying chaotically in both amplitude and frequency. Therefore, the trajectories produced are hard to predict in

the chaotic sense, but remain trackable by naive participants. Dimensions x_3 , x_4 , and x_5 comprise a standard Rössler oscillator. This chaotic system then drives the stiffness of a simple harmonic oscillator, dimensions x_1 and x_2 . For all trials, $a = b = 0.1$, $c = 14$, $\alpha = 100$, and $\beta = 0.3$. The system described by Eq. (11) is then a straightforward extension of simpler systems that might produce more common sinusoidal or linear trajectories.

At the beginning of each trial, a 160-s time series was simulated from initial conditions $x_1 = 1$, $x_2 = 0$, $x_4 = 3.432$, $x_5 = 20.9$, and x_3 taken from a uniform distribution on the interval [18.5, 19.5]. The first 80 s of this time series was truncated in order to remove any transient behavior. Lastly, x_1 was mapped to on-screen coordinates s_x by the mappings in Equation 12.

$$s_x = \frac{(s_{width} - 2s_{xpad})(x_1 - \min x_1)}{\max(x_1 - \min x_1)} + s_{xpad} \quad (12)$$

where $s_{xpad} = 0.25 s_{width}$ and s_{width} is screen width.

While the simulation was displayed on-screen, a stream of dots was constantly emitted from a 10×10 pixel green square, the

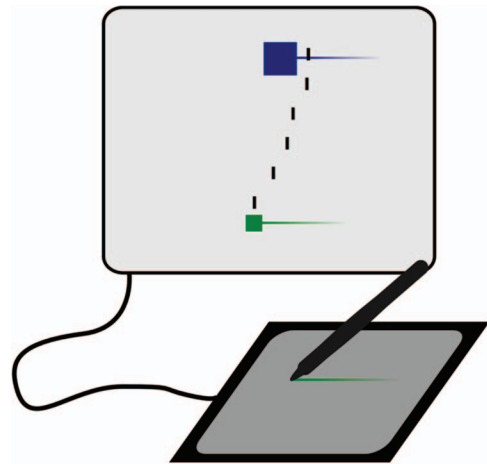


Figure 3. Schematic of the setup in Experiment 1. A cursor (bottom, small square) is controlled by the participant via a stylus and tablet. The cursor emits dots moving upward at various speeds and intervals. The participant’s objective is to intercept the target (top, large square) with as many dots as possible. See the online article for the color version of this figure.

cursor, moving upward at a variable speed and frequency. Participants were instructed to use the stylus and tablet to control the cursor to intercept the target with as many dots as possible. Each time a dot intercepted the target, it briefly changed color to red, and a score was incremented by 5 and displayed immediately above. The time taken for a dot to travel from the cursor to target defines a delay, and therefore an amount of anticipation required to succeed at the task. Typical target and cursor trajectories are displayed in Figure 4.

Delays were randomized within each block from the set $\tau = \{0.1, 0.2, \dots, 0.8\}$ s. Horizontal and vertical coordinates of tablet input, that is, the movement of the hand, were captured as y_1 and y_2 , respectively. As such, the data collected parallel the states x and y of the master-slave system described in Equation 1. Coupling, and subsequently synchronization, is considered to be between the hand and target. The time delay between cursor and target plays the same supporting role as does y_τ from Equation 1. More precisely, when there are multiple dots on screen, each i th dot represents a delay τ_i , where $0 < \tau_i < \tau$.

This is an interesting departure from the coupling function assumed in Stepp (2009). As suggested above, this departure moves the coupling arrangement from the canonical anticipating synchronization class U_0S_1 to U_0S_n , which has an implication for expected results as judged by the aforementioned simulations.¹

Analysis. For the purpose of analysis, the first dimension of the target time series, x_1 , was compared with the first dimension of the participant time series, y_1 . These two dimensions correspond to the horizontal movements of each. To determine both the level of synchrony, ρ , and amount of phase shift, τ^* , between x_1 and y_1 we used the maximum of the cross-correlation between the two (Stepp & Frank, 2009).

For each trial, these two quantities were calculated according to Equation 13,

$$\rho = \text{xcorr}_{x,y}(\tau^*) = \max_{\tau} \text{xcorr}_{x,y}(\tau) \quad (13)$$

where $\text{xcorr}_{x,y}(\tau)$ is the normalized cross-correlation function of x_1 and y_1 with lags from the interval $\tau = [-40, 40]$.

A second way to describe anticipatory performance is to not measure observed τ^* at all, but compare x and y_τ directly. Using τ^* as our lag of interest, we may attain a high ρ if the participant is synchronizing well at *some* delay (namely τ^*). This is not directly related to succeeding at the task, however. A correlation, ρ_τ , between x and y_τ gives a direct measurement of this.

Each participant produced three blocks of eight time series such that each (τ, k) condition was repeated three times. Whereas the first block was considered practice and not analyzed, the second two blocks were analyzed using the methods above to generate ρ , ρ_τ , and τ^* measures for each trial. Participants in similar tasks (Miall & Jackson, 2006) have shown adaptation across many trials. In the case of the current task, however, differences between participant performance in Block 2 and Block 3 were not significant, as tested by a paired-sample t test on ρ and τ^* values between the two blocks ($\rho: t(15) = 1.0234, p = .3233$; $\tau^*: t(15) = -1.3129, p = .2090$). As such, analyses below are conducted using mean values per participant. Given our measures, we may examine the effect of τ on each in turn.

Results

Figure 5 depicts ρ , ρ_τ , and τ^* measures as described above. The dependence of these measures on τ are strikingly contrary to the expected behavior seen in Stepp (2009) and predicted by simulations in the class U_0S_1 (for simulations see Stepp & Turvey, 2010). Comparing with Figure 1, this deviation appears consistent with predictions from simulations of the more general class U_0S_n , which matches the coupling arrangement used in this experiment.

A linear regression of τ^* on $\tau < 500$ ms shows a linear fit ($R_2 = 0.7602, F(1, 50) = 158.5, p < .001$) with slope 0.49 (CI: [0.4157, 0.5735]). A linear regression of ρ on τ shows a moderate linear fit ($R_2 = 0.5432, F(1, 102) = 121.3, p < .001$) with slope -0.2051 (CI: $[-0.2420, -0.1682]$), but not a cubic fit (b_3 CI: $[-0.8505, 1.1324]$).

Discussion

In Stepp (2009), comparisons were made between standard features of simulated anticipating synchronization and the synchronization behavior of participants in a manual tracking experiment. In the present experiment, however, the structure of delayed feedback is different due to the possibility of multiple feedback delays. Employing the notation from Stepp and Turvey (2015), the present experiment comes from the more general class U_0S_n , and its empirical results show a relatively linear dependence of ρ on τ , seemingly without a critical region where synchrony breaks down. As explored below, increased stability for larger values of τ is a prediction from simulation. It is feasible that extending the range of delay would result in finding that critical region—a hypothesis that warrants further study.

¹ Fluctuations in a system with a single delay might present as a system with multiple delays, but only for carefully designed fluctuations. Adding Gaussian or uniform noise to a U_0S_1 system does not result in the same phenomenology as a U_0S_n system.

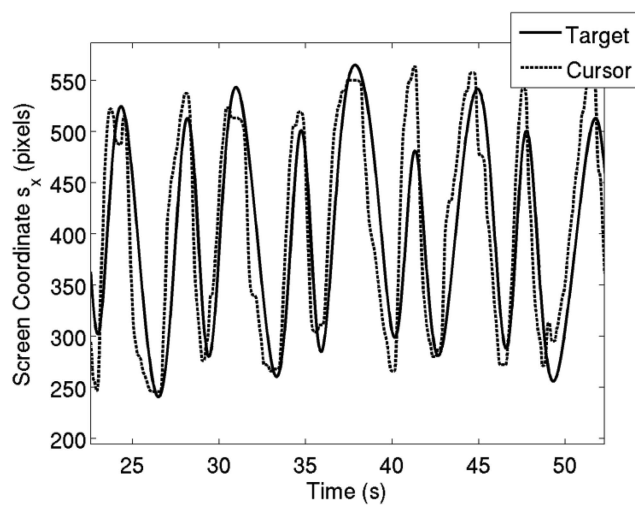


Figure 4. Sample time series from Experiment 1. The target horizontal screen coordinate (solid) follows a chaotic oscillator. Cursor position (dashed) shows the participant's movements, which are shown here leading the target.

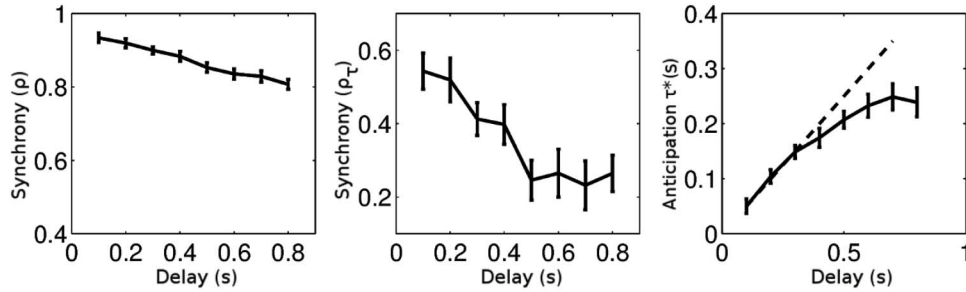


Figure 5. Cross-correlation analysis of participant data. Plots show ρ , ρ_c , and τ^* from left to right.

The results from this experiment serve an important role connecting the generalized theory of anticipating synchronization to human anticipatory behavior. Although experiments such as Stepp (2009) establish consistency with anticipating synchronization, those results in combination with the results of the present Experiment 1 establish a much firmer predictive landscape. Employing other modeling techniques, especially those requiring an internal model of the anticipated system, are much less likely to replicate this pattern. Instead, we see that both behaviors observed in Stepp (2009) and in the present experiment are predicted by some process of synchronization relatively similar to those described in *Coupling scheme* and *Simulations* above, most importantly, following the same alterations to the coupling arrangement.

Experiment 2

Although manual tracking experiments such as Stepp (2009) and Experiment 1 are clearly anticipatory and closely match prior anticipating synchronization arrangements, they are somewhat artificial. This artificiality helps connect empirical results to formal expectations, but more natural settings should be investigated as well.

Navigating over a path at some speed is such a natural setting. Given that it is a problem faced by all animals, it can be considered fundamental. Not only is this task fundamental, it is also anticipatory, entailing traveling at speed with delayed action. In order to probe this task in humans, a driving study was conducted focusing on the interplay between control delay and anticipation.

Method

Participants. Eight students at the University of Connecticut participated in this study. The participants were three women and five men, either undergraduate or graduate students. All eight were right-handed as defined by the hand with which the participant preferred to draw. Participants gave informed consent and, in the case of the undergraduates, received class credit for their voluntary participation. The study was approved by the University of Connecticut Institutional Review Board.

Apparatus. A computer display (39 cm diagonal, 1024×768 pixel resolution) was positioned at a distance of approximately 26.7 cm ($SD = 8.8$ cm) from screen to eye. A pressure sensitive tablet (18 cm diagonal) sat 25 cm in front of the same display, although participants were free to move it to remain comfortable. Participants held a 14 cm stylus in their dominant hand that they could position on the tablet in order to interact with the display.

The tablet and stylus were visible to the participant. The experiment setup is depicted in Figure 6.

Participants viewed a rudimentary driving simulator created using the VisionEgg, PyGame, and PIL Python modules. A typical view in the simulator is depicted in Figure 7. Using the hand-held stylus, participants could control the visible steering wheel. Horizontal position of the stylus on the tablet was mapped to a steering angle, θ , on the interval $[-\frac{\pi}{2}, \frac{\pi}{2}]$ radians. This angle was used to rotate the steering wheel during the simulation and also to set the turning rate (rad/s) of an invisible virtual vehicle traveling with a constant speed, v . Within the simulator, a configurable delay, τ , could be added between steering angle and its effect on heading direction.

Eight winding roads were created from the x_1 state of Equation 11. To generate a road, the system was simulated for 120 s with an x_3 initial state chosen from a uniform random distribution $U(18.0, 19.0)$. The last 60 s of the x_1 time series was then used as the road path. To create a road with a left and right side, this path was copied and shifted by 0.5 and then both curves were normalized to lie within the interval $[0, 100]$.

To construct an actual simulation, a road time series was read from a text file and a 2000×100 pixel image of the road was created. The simulator screen was partitioned into sky and ground

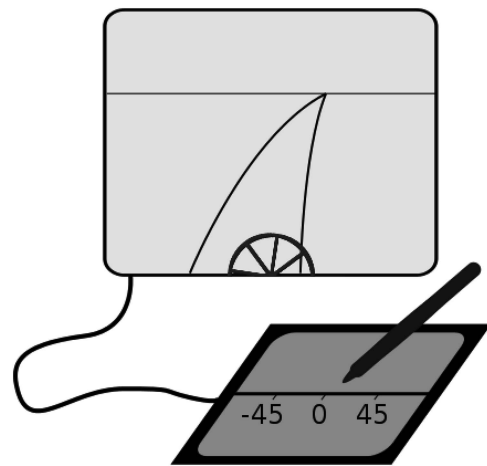


Figure 6. Schematic of the setup in Experiment 2. A simple driving simulator displayed on a computer screen, along with a participant-controlled steering wheel. The angle of the steering wheel corresponds to the position of the stylus on the tablet.

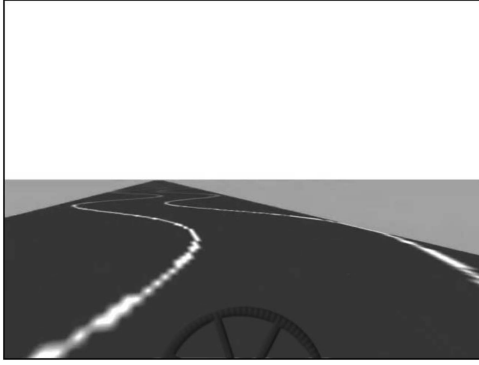


Figure 7. Screenshot from the driving simulator, showing the road laid out ahead of the driver, and a small steering wheel to indicate current turning rate.

on the top half and the bottom half of the screen, respectively. Onto this partitioning the road image was projected using a perspective transform so that it vanished at the horizon. It is worth noting at this point that viewing the upcoming road is tantamount to access to upcoming states of the road. That is, with a single delayed feedback between driver and virtual vehicle, these upcoming, essentially future, states of the road match anticipating synchronization class $U_{\infty}S_1$.

Eye tracking. Before using the simulator, each participant was situated for eye-tracking using an SR Research EyeLink II eye tracking system (SR Research, Ottawa, Ontario, Canada). Preparation consisted of a standard EyeLink calibration routine started from within the driving simulator. Between each trial, calibration was checked and the participant recalibrated if the check failed.

Procedure. Before completing any experimental trials, participants were given three practice trials, each lasting 60 s. During these trials, no external delay was applied to the steering mechanism. Once familiar with the simulator in general, 16 trials were presented in a randomized order. For each trial, a delay was inserted between the movement of the on-screen steering wheel and the effect that steering angle had on the virtual vehicle heading. These delays were taken from the set $\tau = \{0.05, 0.1, \dots, 0.8\}$ s. Once the participant signaled readiness, the simulator was started and the participant attempted to steer so as to remain in between the two lines of the virtual road (see Figure 7). After 60 s, the simulator stopped and the participant was allowed to rest for as long as desired. Upon initiation of the following trial, eye-tracker calibration was checked and the next simulator run began.

Analyses. In this experiment there were three primary functions of interest, corresponding to eye (E), hand (H), and road (R). We may think of corresponding time series, $E(t)$ and $H(t)$, developing over time within a trial, and $R(z)$ over spatial variable z . In addition to these primary time series, there are several secondary time series of interest, virtual vehicle position (V), virtual vehicle turning rate (Θ), virtual vehicle heading direction (D), and derivatives of $R(z)$. In cases where a time series has multiple components, a subscript may be used to identify a specific one, for instance $H_x(t)$ denotes the x -coordinate of $H(t)$. During the course of a trial, the participant was, in essence, asked to coordinate these three functions in a particular way. As such, we wish to examine the coordination, or synchronization, between each pair of

time series. Each time series has certain characteristics described below.

The road time series, $R(z)$, was produced by the first dimension of the now standard chaotic-spring system described by Equation 11. A positive and negative bias was added to $R(z)$, which was then normalized to lie within $[0, 100]$ in order to create an enclosed road-like strip as in Figure 8. Coordinates in this world-space are (x', z) . Spatial derivatives over z , $\dot{R}(z)$ and $\ddot{R}(z)$, take on the meanings of road heading and turning rate respectively.

When presented to the participant, $R(z)$ underwent a transform composed of a rotation and translation according to the participant's virtual heading and position on $R(z)$ and a perspective transform mapping $R(z)$ to a display-space with (x, y) coordinates on a viewing plane. These mappings are schematized in Figure 9. The eye time series, $E(t)$, exists in the display-space. Likewise, we can use the reverse perspective transform in order to achieve an $E(z)$. Raw $E(t)$, however, consists of gaze position on the (x, y) viewing plane over time.

Finally, the hand time series, $H(t)$, consisted of the location over time of a hand-held stylus on a pressure-sensitive tablet. This 2D coordinate system was set to be the same as the viewing plane, but was mapped to an angle, $\Theta(t)$, by the following mapping,

$$\Theta(t) = \frac{\pi H_x(t) - m}{2m} \quad (14)$$

where m is half of the viewing plane width. In order to replicate the act of steering, $\Theta(t)$ was taken to be a rotation rate in radians per second.

During the course of the simulation, $\Theta(t)$ was integrated to produce a virtual heading, $D(t)$. A velocity vector was composed of this heading and a constant speed in world units, v , and further integrated to produce a virtual position, $V(t)$. In consequence, the position time series $V(t)$ was a time series of (x', z) coordinates. One can also consider the time series constructed of $V_x(t)$ at the points $V_z(t)$, which is then directly comparable to $R(z)$.

The combination and coordination of $E(t)$, $H(t)$, and $R(z)$ allows for a situation in which multiple slave systems are being driven by one master. Such arrangements have been studied in general and with specific application to circadian synchronization by Stepp and Turvey (2010) and Stepp et al. (2011). It is also conceivable, however, that a nested arrangement exists, for instance that $R(z)$ serves as master for $E(t)$, which in turn serves as master for $H(t)$. Lastly, there may even be a combination of these arrangements such as a $R(z)$ — $E(t)$ hybrid serving as master for $H(t)$.

Results

Hand-road system. Of the time series described above, $R(z)$ is the only one that can be considered an independent variable. In the language of coupled time series it also acts as a master system.

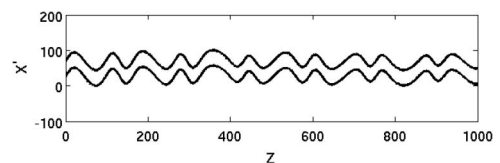


Figure 8. Road time-series $R(z)$ generated from Equation 11.

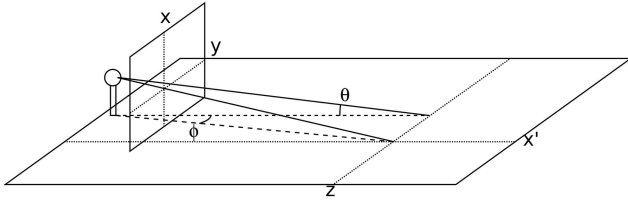


Figure 9. Perspective mapping between simulation display and virtual road. Display coordinates x and y are transformed to ground coordinates x' and z . Because the ground coordinate system is also two dimensional, the reverse transform is possible.

As described above, the instructed task for the participant was to stay between the lines of the road as best as possible. That is, maintain synchrony between $V_x(t)$ and $R(V_z(t))$. Synchrony plots, the familiar ρ and τ^* measurements, for this pair are shown in Figure 10. Participants had, however, only one way to control $V(t)$, which was by controlling the turning rate $\Theta(t)$. Therefore, the control problem for the participant was to maintain synchrony between $\Theta(t)$ and $\ddot{R}(V_z(t))$, that is to match the turning rate of their vehicle to the turning rate of the road. Synchrony plots for this pair are shown in Figure 11.

Figure 11 allows for comparison with standard features of anticipating synchronization (Voss, 2000; Stepp, 2009). The measures ρ and τ^* show distinctive features in their relation to τ . Specifically, anticipating synchronization dynamics predict a cubic shape for ρ , a low-variability linear relationship of τ^* to small

values of τ , and sudden high-variability and weak relationship of τ^* to values of τ past some critical region. In the experiments of Stepp (2009), this critical region appeared to be between 0.4 and 0.6 s. Each of these features exists in Figure 11. A linear regression of ρ on powers of τ up to degree 3 shows a cubic shape ($R^2 = 0.96031$, $F(1, 126) = 96.7831$, $p < .001$, b_3 CI: [0.5196, 3.805]). Values of τ^* show a linear relationship the values of τ below 0.5 s ($\tau \leq 300$ ms: $R^2 = 0.9629$, $F(1, 38) = 103.8268$, $p < .001$; $\tau \leq 500$ ms: $R^2 = 0.71872$, $F(1, 78) = 20.4415$, $p = .0019467$), at which point there is a sudden jump in variability (see Figure 11).

In contrast to Figure 11, Figure 10 is a metric of performance of the task goal, but is not directly related to anticipating synchronization. As such it shows *some* of the features of anticipating synchronization, but only weakly so. A linear regression of ρ up to a cubic term fits the data well ($R^2 = 0.95199$, $F(1, 14) = 79.3112$, $p < .001$), but the cubic term does not contribute significantly to the overall model (b_3 CI: [-0.8146, 3.524]). Values of τ^* at or below τ of 300 ms show a linear relationship ($R^2 = 0.93138$, $F(1, 4) = 54.2922$, $p = .0018078$), but those at or below 500 ms do not ($R^2 = 0.0057061$, $F(1, 8) = 0.045911$, $p = .8357$).

Eye-road system. The behavior of the eyes while driving has been studied previously (Kim & Turvey, 1999; Land & Horwood, 1995; Land & Lee, 1994; Wilkie, Wann, & Allison, 2008). In Land and Lee (1994), two drivers in real-world conditions drove down a winding road while their gaze locations and steering angles were tracked. In terms of Table 1, $R(z)$ is defined by a real roadway, and data collected corresponded to $E(z)$ and $D(t)$. Data from Driver 1 of this study is reproduced in Figure 12.

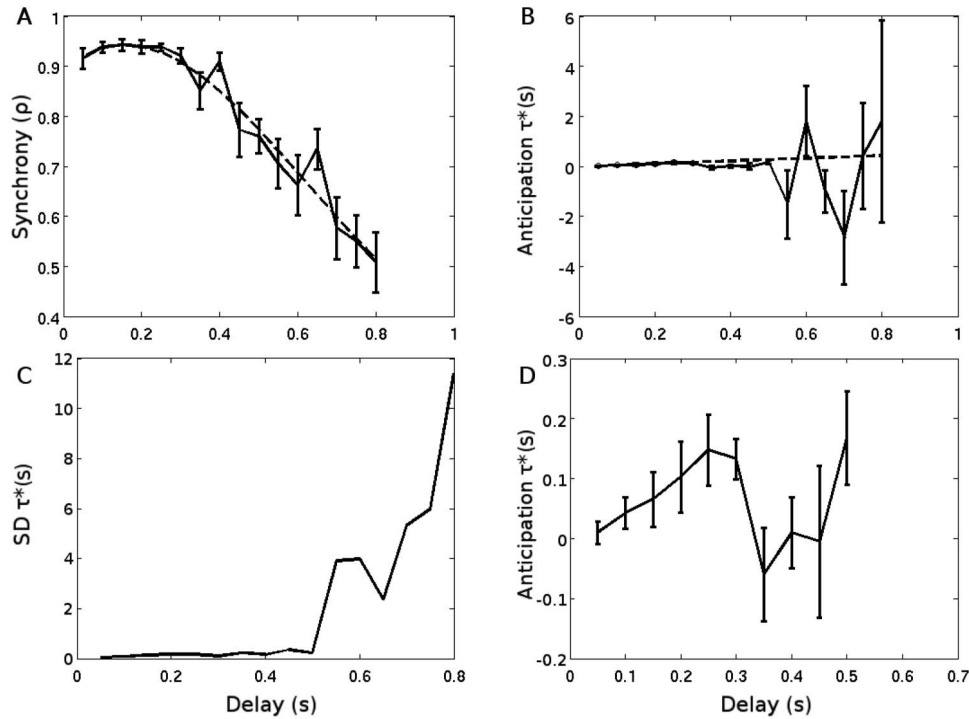


Figure 10. Cross-correlation analysis comparing $V_x(t)$ and $R(V_z(t))$. This pair encapsulates the task goal presented to the participant. Panel A: Maximum cross-correlation. Panel B: Time shift at maximum cross-correlation. Panel C: Standard deviation of time shifts across participants. Panel D: initial range of time shift. Time shifts here are represented in ground units.

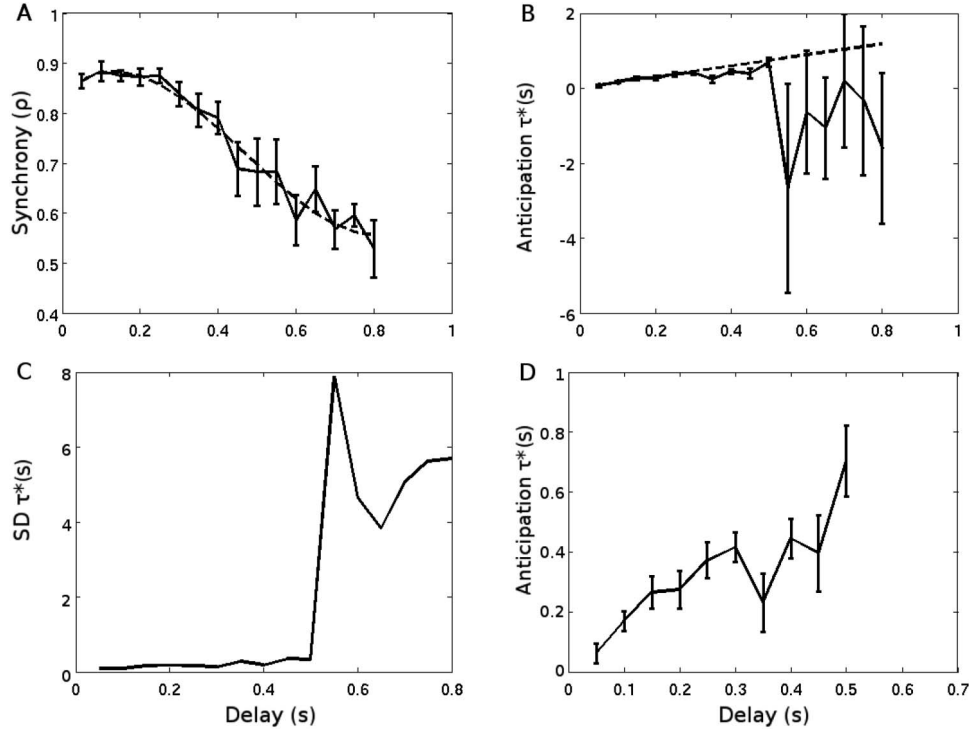


Figure 11. Cross-correlation analysis comparing $\Theta(t)$ and $\dot{R}(V_z(t))$. This pair closely matches the control problem presented to the participant. Panel A: Maximum cross-correlation. Panel B: Time shift at maximum cross-correlation. Panel C: Standard deviation of time shifts across participants. Panel D: Initial range of time shift. Time shifts here are represented in ground units.

Comparing Figure 12 with Figure 13, the data from the simulator used in this study, it appears that drivers in this simulated environment behaved similarly to Land and Lee’s drivers. That is, gazes fell on the upcoming turns, and steering angle followed the road. Land and Lee (1994) showed that drivers look at the road tangent point. This is also true within the simulated environment, although it appears differently in Figure 13 than in Figure 12. The difference is due to the portion of road visible in each case.

Approaching the Eye–Road system as before, we may conduct a usual cross-correlation analysis. Comparing the road and gaze time series using a cross-correlation is nontrivial because gazes do not extend monotonically along the road, but move back and forth in the z direction. One way to compare eye and road is to take the vehicle position at each point along the road and ask at what x'

coordinate is the gaze location. That is, construct a time series using the z coordinate of $V(t)$ and the x' coordinate of $E(z)$. This time series is then compared with $R(z)$. Plots of ρ and τ^* for this comparison are shown in Figure 14.

Coupling between these two time series is not the type of anticipating synchronization described in Experiment 1. Nevertheless, the cross-correlation analysis does show temporal relationships and synchrony. Unless the driver is looking straight down, gaze location $E(z)$ is always ahead (greater z coordinate) of $V(t)$. This shows up in Figure 14 as a bias toward anticipatory τ^* . A notable departure from usual patterns in the τ^* plot is a near constant shift until synchronicity breaks down.

Discussion

The driving simulator developed for this study provides for a minimal driving environment and means to manipulate control delay. Regardless of its simplicity, the simulator generates a rich data set as summarized in Table 1. Together, these time series allow for detailed analysis of the eye–hand–road system in the presence of control delay. Although comparison between any of the time series in Table 1 is possible, there are a few that are more interesting than others, especially when investigating the relationship of empirical data to theoretical expectations.

As described above, a participant in Experiment 2 had a single degree of freedom to control, namely, the turning rate of the virtual vehicle. To stay on the road, the control problem was to match this turning rate to the turning rate of the road at the current vehicle

Table 1

Primary and Secondary Time-Series for Road, Hand, and Eye

Time-Series	Coordinates	Description	Derivation
$H(t)$	display— (x, y)	Stylus (hand) position	Participant
$\Theta(t)$	ground— (θ)	Vehicle turning rate	$(\pi/2)(H_x(t) - m)/m$
$E(t)$	display— (x, y)	Gaze position	Participant
$D(t)$	ground— (ϕ)	Vehicle heading	$\int \Theta(t) dt$
$V(t)$	ground— (x', z)	Vehicle position	$\int v D(t) dt$
$R(z)$	ground— (x')	Road shape	Experimenter
$\dot{R}(z)$	ground— (x'/z)	Road heading	dR/dz
$\ddot{R}(z)$	ground— (x'/z^2)	Road turning rate	$d\dot{R}/dz$

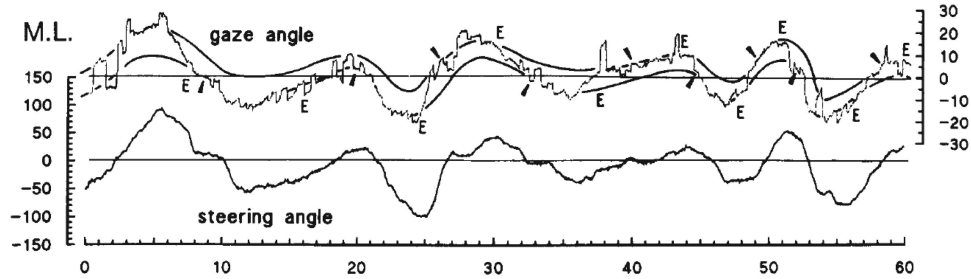


Figure 12. Gaze and steering angle data for a driver in a real driving setting. Reproduced from Land and Lee (1994).

position. It is this comparison that showed the greatest correspondence to properties of anticipating synchronization, as detailed above. It was the case, however, that the coupling structure of the present experiment was not of the single master time, single delay type. Instead, as noted above, coupling was also made to upcoming values. Simulations were conducted which match this type of coupling, for different delay times and different amounts of upcoming values. These simulations help to weave together the phenomenology seen in the time-series comparisons in Figures 8 and 11, that being the $\Theta(t)$ and $\dot{R}(V_z(t))$ pair and the $E(z)$ and $R(z)$ pair. The shape of Figure 11a was expected from typical anticipation synchronization behavior, but the τ^* plot in Figure 11d shows a much increased anticipation (anticipation by more than the imposed delay τ). A second unexpected feature was that the phase shift between eye and road time series was constant for changing τ . Both of these properties are expected when taking into account the effect of coupling to upcoming values. As seen in the simulated τ^* plot of Figure 4b, τ^* increases with increasing τ at a slope greater than one. Additionally, there is a look-ahead value at which anticipation is maximized across values of τ . This last feature suggests that a constant shift between eye and road is also expected, if gaze direction functions to maximize anticipation. Clearly these statements deserve further study to move past the point of conjecture, but the theoretical predictions identified herein make them plausible enough to do so.

General Discussion

We have generalized the delay-coupling arrangement from Voss (2000) to accommodate different numbers and types of time-shifted couplings. This generalization helps to define classes of

systems based on type of coupling. A notation labels the classes $U_m S_n$, according to the number (m and n) of time-shifted couplings to points in the driver (U) or driven (S) system. Simulations of these classes using the Rössler–Spring system show particular behaviors for the different classes of couplings. Empirical results for class $U_0 S_1$ had already shown agreement with theoretical expectations (Stepp, 2009). In the present research, empirical results for classes $U_0 S_n$ and $U_\infty S_1$ likewise met the theoretical expectations.

At this juncture it is prudent to ask what these results mean and what they do not mean. The present research was not aimed at bettering inference-based anticipation (e.g., Rosen, 2012). It was aimed at the issue of whether variations in the phenomenology of real anticipatory behavior can be explained by a dynamical system that does not rely on predictions from a small-scale model. Of significance is not that anticipation grounded in nonlinear dynamics works better than inference-based anticipation, but that it works at all.

An obvious benefit of anticipation as dynamical rather than inferential is the promise of an understanding of anticipatory behavior that applies to all phyla (cf. Stepp & Turvey, 2010). That is, an understanding of anticipation at the level of general principle. Given such, one would expect that organisms would necessarily be anticipatory, to greater or lesser degree. Anticipation is another way of synchronizing, which is a phenomenon already known to happen opportunistically (Pikovsky, Rosenblum, & Kurths, 2001).

The manual tracking task of the present experiments differed from the experiment of Stepp (2009). Participants in the present Experiments 1 and 2 were similarly asked to synchronize with the current state of a master time series, but instead of receiving feedback at a

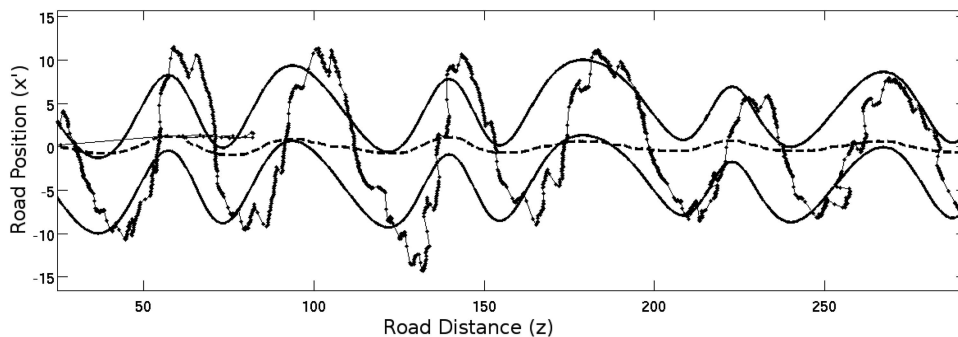


Figure 13. Gaze location (solid) and steering angle data (dashed) from a simulated driving session.

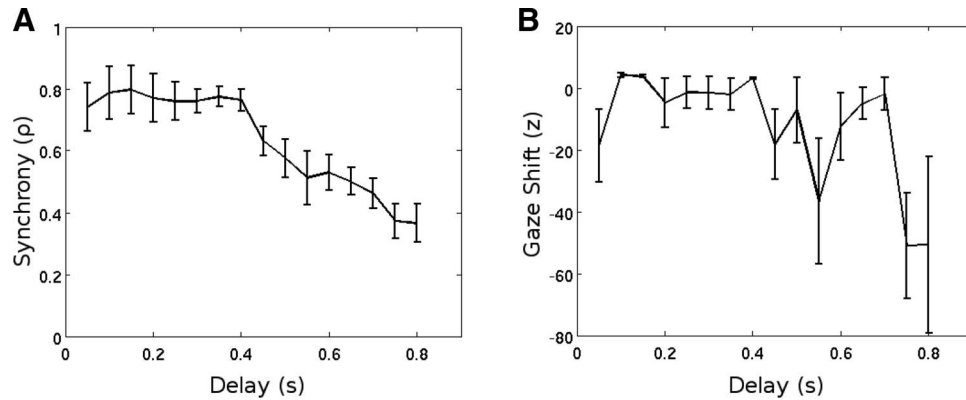


Figure 14. Cross-correlation analysis of $R(z)$ and $E(z)$ at z values given by $V_z(t)$. Panel A: Maximum cross-correlation. Panel B: Gaze shift at maximum cross-correlation.

single delay, feedback was presented at multiple delay times. This change is analogous to changing from class U_0S_1 to U_0S_n with $n > 1$. Figure 1 shows how the Rössler–Spring system reacts to such a change, which was mirrored qualitatively by participant behavior. Specifically, anticipating synchronization is stable at longer delay times, apparently due to multiple delays, and anticipation makes up for approximately 40%–50% of the imposed delay. It is this particular combination of features that matches participant behavior. It is possible to achieve individual features by other arrangements. For instance, longer anticipation times are attainable through various networks of dynamical systems (Wang, Huang, & Qi, 2005). Networked systems, especially recurrent networks, offer an intriguing model for the study of multiple feedback delays. Each cycle in the network (a path that meets itself) corresponds to a delay according to its length. A sufficiently connected network contains a large number of cycles, allowing for a large distribution of possible delays.

Experiment 2, at least in abstraction, is also a deviation from the U_0S_1 class, this time adding coupling to not just the present state of a master time series, but to a section of upcoming values. This type of coupling is also simulated in Experiment 1 for a Rössler–Spring system, and qualitative features are replicated. The constant shift in Experiment 2 between gaze and road is predicted by there being a particular look-ahead value that maximizes anticipation. Furthermore, anticipation with coupling to upcoming values is expected to increase at a greater rate than imposed delay.

The foregoing, as implied at the start, qualifies as an investigation of a coupling-anticipation relation, as opposed to a representation-anticipation relation. Extremely simple organisms show anticipatory behavior (e.g., Saigusa, Tero, Nakagaki, & Kuramoto, 2008), which is more simply explained if there is no need to also explain mechanisms for building and utilizing internal models. It is simpler to find principles that allow anticipatory behavior to arise naturally in a physical system. We take the above as evidence that the persistent phenomenon of synchronization might underlie such a principle.

References

Atay, F., & Karabacak, Ö. (2006). Stability of coupled map networks with delays. *SIAM Journal on Applied Dynamical Systems*, 5, 508–527. <http://dx.doi.org/10.1137/060652531>

- Dubois, D. M. (2003). Mathematical foundations of discrete and functional systems with strong and weak anticipations. In M. V. Butz, O. Sigaud, & P. Gérard (Eds.), *Anticipatory behavior in adaptive learning systems* (pp. 110–132). Berlin, Germany: Springer. http://dx.doi.org/10.1007/978-3-540-45002-3_7
- Fink, P. W., Foo, P. S., & Warren, W. H. (2009). Catching fly balls in virtual reality: A critical test of the outfielder problem. *Journal of Vision*, 9, 1–8.
- Foulkes, A., & Miall, R. (2000). Adaptation to visual feedback delays in a human manual tracking task. *Experimental Brain Research*, 131, 101–110.
- Gibson, E. J. (1994). Has psychology a future? *Psychological Science*, 5, 69–78
- Kim, N., & Turvey, M. T. (1999). Eye movements and a rule for perceiving direction of heading. *Ecological Psychology*, 11, 233–248. http://dx.doi.org/10.1207/s15326969eco1103_3
- Land, M., & Horwood, J. (1995). Which parts of the road guide steering? *Nature*, 377, 339–340. <http://dx.doi.org/10.1038/377339a0>
- Land, M. F., & Lee, D. N. (1994). Where we look when we steer. *Nature*, 369, 742–744. <http://dx.doi.org/10.1038/369742a0>
- Miall, R. C., & Jackson, J. K. (2006). Adaptation to visual feedback delays in manual tracking: Evidence against the Smith Predictor model of human visually guided action. *Experimental Brain Research*, 172, 77–84. <http://dx.doi.org/10.1007/s00221-005-0306-5>
- Michaels, C. F., & Oudejans, R. R. (1992). The optics and actions of catching fly balls: Zeroing out optical acceleration. *Ecological Psychology*, 4, 199–222. http://dx.doi.org/10.1207/s15326969eco0404_1
- Pikovsky, A., Rosenblum, M., & Kurths, J. (2001). *Synchronization: A universal concept in nonlinear sciences*. New York, NY: Cambridge University Press. <http://dx.doi.org/10.1017/CBO9780511755743>
- Rosen, R. (2012). *Anticipatory systems: Philosophical, mathematical, and methodological foundations* (Vol. 1). New York, NY: Springer Science & Business Media.
- Saigusa, T., Tero, A., Nakagaki, T., & Kuramoto, Y. (2008). Amoebae anticipate periodic events. *Physical Review Letters*, 100, 018101. <http://dx.doi.org/10.1103/PhysRevLett.100.018101>
- Saxberg, B. V. (1987). Projected free fall trajectories: I. Theory and simulation. *Biological Cybernetics*, 56, 159–175. <http://dx.doi.org/10.1007/BF00317991>
- Stapp, N. (2009). Anticipation in feedback-delayed manual tracking of a chaotic oscillator. *Experimental Brain Research*, 198, 521–525. <http://dx.doi.org/10.1007/s00221-009-1940-0>
- Stapp, N., Chemero, A., & Turvey, M. T. (2011). Philosophy for the rest of cognitive science. *Topics in Cognitive Science*, 3, 425–437. <http://dx.doi.org/10.1111/j.1756-8765.2011.01143.x>

- Stepp, N., & Frank, T. D. (2009). A data-analysis method for decomposing synchronization variability of anticipatory systems into stochastic and deterministic components. *European Physical Journal: B. Condensed Matter Physics*, *67*, 251–257.
- Stepp, N., & Turvey, M. T. (2010). On strong anticipation. *Cognitive Systems Research*, *11*, 148–164. <http://dx.doi.org/10.1016/j.cogsys.2009.03.003>
- Stepp, N., & Turvey, M. T. (2015). The muddle of anticipation. *Ecological Psychology*, *27*, 103–126. <http://dx.doi.org/10.1080/10407413.2015.1027123>
- Turvey, M. T. (2013). Ecological perspective on perception–action: What kind of science does it entail? In W. Prinz, M. Bessard, & A. Herwig (Eds.), *Action science: Foundations of an emerging discipline* (pp. 139–170). Cambridge, MA: MIT Press. <http://dx.doi.org/10.7551/mitpress/9780262018555.003.0006>
- Turvey, M. T. (2015). Quantum-like issues at Nature’s Ecological Scale (the scale of organisms and their environments). *Mind and Matter*, *13*, 7–44.
- Vercher, J. L., & Gauthier, G. M. (1992). Oculo-manual coordination control: Ocular and manual tracking of visual targets with delayed visual feedback of the hand motion. *Experimental Brain Research*, *90*, 599–609. <http://dx.doi.org/10.1007/BF00230944>
- Voss, H. U. (2000). Anticipating chaotic synchronization. *Physical Review: E. Statistical Physics, Plasmas, Fluids, and Related Interdisciplinary Topics*, *61*, 5115–5119. <http://dx.doi.org/10.1103/PhysRevE.61.5115>
- Voss, H. U., McCandliss, B. D., Ghajar, J., & Suh, M. (2007). A quantitative synchronization model for smooth pursuit target tracking. *Biological Cybernetics*, *96*, 309–322. <http://dx.doi.org/10.1007/s00422-006-0116-2>
- Wang, H. J., Huang, H. B., & Qi, G. X. (2005). Long-time anticipation of chaotic states in time-delay coupled ring and linear arrays. *Physical Review: E. Statistical, Nonlinear, and Soft Matter Physics*, *71*, 015202. <http://dx.doi.org/10.1103/PhysRevE.71.015202>
- Wilkie, R. M., Wann, J. P., & Allison, R. S. (2008). Active gaze, visual look-ahead, and locomotor control. *Journal of Experimental Psychology: Human Perception and Performance*, *34*, 1150–1164. <http://dx.doi.org/10.1037/0096-1523.34.5.1150>

Received August 11, 2016

Revision received December 29, 2016

Accepted January 2, 2017 ■